

# The Impact of Hurricane Force Wind Fields on the North Pacific Ocean Environment

STEVEN BUSINGER, SELEN YILDIZ, AND THOMAS E. ROBINSON

*University of Hawai'i at Mānoa, Honolulu, Hawaii*

(Manuscript received 9 September 2014, in final form 30 January 2015)

## ABSTRACT

This study analyzes QuikSCAT surface wind data over the North Pacific Ocean to document the distribution of captured fetches in extratropical cyclones that produced hurricane force (HF) wind fields from January 2003 through May 2008. A case study is presented to introduce the datasets, which include surface wind analyses from the Global Forecast System (GFS) Global Data Assimilation System (GDAS), and wave hindcasts from the third-generation wave model (WAVEWATCH III; hereafter, WW3), in addition to the QuikSCAT surface wind data. The analysis shows significant interannual variability in the location of the captured fetches as documented by QuikSCAT, including a shift in the distribution of captured fetches associated with ENSO. GDAS surface winds over the ocean are consistently underanalyzed when compared to QuikSCAT surface winds, despite the fact that satellite observations of ocean surface winds are assimilated. When the WW3 hindcasts associated with HF cyclones are compared with buoy observations over the eastern and central North Pacific Ocean, the wave model significantly underestimates the large-swell events.

## 1. Introduction

Extratropical cyclones producing extreme surface wind conditions are ubiquitous over the oceans during winter. Winds with speeds in excess of  $20 \text{ m s}^{-1}$  are observed more than 10% of the time within broad swaths of the storm tracks located over the western and central North Pacific, and over the North Atlantic to the north of  $30^\circ\text{N}$  (Sampe and Xie 2007). The number of storms producing hurricane force (HF) winds (speeds greater than  $32.9 \text{ m s}^{-1}$ ) is generally greater than 20 per season over the North Pacific and North Atlantic Oceans to the north of  $30^\circ\text{N}$  (e.g., Fig. 1). This number may be greater than 50 during more-active years (e.g., Von Ahn et al. 2005; Jelenak et al. 2009). Extreme surface wind conditions typically exist over larger areas (Dickinson and Brown 1996) and over longer periods than in tropical cyclones (Willis et al. 2004).

These winds in turn influence ocean surface wave characteristics (Wang and Swail 2001). In particular, variability in extreme wave conditions is related to variability in atmospheric circulation patterns (e.g., frequency and intensity of extratropical cyclones)

(Izaguirre et al. 2011). From the perspective of individual cyclones, large ocean waves may form and propagate over long distances depending on the storm's wind speed and fetch characteristics (Jelenak et al. 2009; Caldwell and Aucan 2007). A fetch has alternatively been defined as the length or area of open water over which winds blow in an essentially constant direction. A captured fetch is a circumstance during which the storm motion is in the same direction as the fetch, thus keeping enhanced storm winds over the growing wave field. The largest wind waves are associated with captured fetches (Butt et al. 2014). Extremely large waves present an enormous threat to the safety of all marine operations, including but not limited to cargo shipping, passenger cruises, offshore oil platform operations, and search and rescue missions (Kite-Powell 2011). A combination of high winds and associated extreme wave conditions may result in loss of cargo, vessels, and lives. Hurricane force wind fields can also cause hazardous and destructive conditions along coastlines thousands of miles away (Caldwell and Aucan 2007). Accurate estimates of current and future wind and sea state conditions are critical for safe and efficient operations at sea and along coasts.

After the QuikSCAT satellite was launched in June 1999, the resulting surface wind estimates were incorporated into GDAS starting in July 2001 (Ebuchi et al. 2002). QuikSCAT remotely sensed winds are well behaved in extratropical cyclones because the winds are

---

*Corresponding author address:* Steven Businger, Dept. of Atmospheric Sciences, University of Hawai'i at Mānoa, 2525 Correa Rd., Honolulu, HI 96822.  
E-mail: businger@hawaii.edu

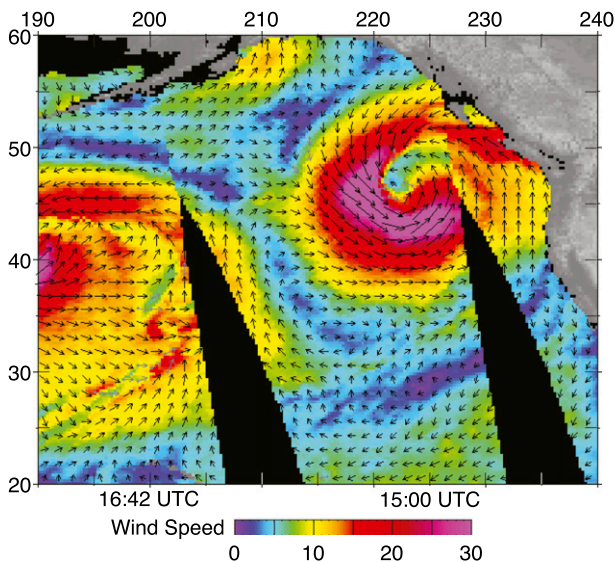


FIG. 1. QuikSCAT winds on 10 Mar 2008 (shading and vectors;  $\text{m s}^{-1}$ ).

on a scale that is well sampled by satellites and the HF wind fields tend to cover rain-free or rain-limited environments (e.g., Fig. 1). This is in contrast to tropical cyclones in which the highest winds are in a narrow band, often obscured by very intense rainfall in the eyewall. In October 2001, the QuikSCAT data were made available to the National Oceanic and Atmospheric Administration's (NOAA) Ocean Prediction Center (OPC) forecasters, who are responsible for marine warnings, forecasts, and guidance for maritime users (Chang et al. 2009). The OPC's warning bulletins are required to be received and monitored by all American commercial vessels of 300 gross tons or greater operating in the North Atlantic and North Pacific Oceans' (to the east of  $160^{\circ}\text{W}$ ) high seas and offshore waters (Jelenak et al. 2009). With its 1800-km-wide swath, large retrievable wind speed range, and rapid data delivery, QuikSCAT revolutionized short-term warning and forecasting over the expansive ocean area of responsibility covered by the OPC. According to a study in the fall of 2002, when QuikSCAT winds were used in the forecast process, the number of marine wind warnings increased by 30% (Von Ahn et al. 2006). The warning category of HF was added in December 2000, once it became clear that QuikSCAT was able to consistently detect HF conditions. Prior to QuikSCAT, OPC forecasters relied on infrequent ship observations in the open ocean with no way to consistently detect or warn for these HF storms. The current literature on HF extratropical cyclone climatology is limited to the studies of Von Ahn et al. (2005) and Jelenak et al. (2009). These studies provide statistics on their distribution,

longevity, deepening rate, central pressure, and the average wind speed distribution in the cyclones.

At any given time, the Pacific Ocean contains numerous temporally and spatially evolving wave systems originating from a wide variety of wind-generation events (Hanson et al. 2009). The waves generated by these storms can exceed 30 m (100 ft) in the open ocean (Jelenak and Chang 2008). The challenge for numerical wave models, such as the third-generation wave model (WAVEWATCH III; hereafter, WW3; Tolman 2002b), is to estimate and forecast the nonlinear rapid evolution of the complex ocean wave field. There have been several validation studies comparing version 2.22 of the WW3 to the National Data Buoy Center (NDBC) buoys of NOAA in the North Pacific Ocean (Tolman 2002b; Stopa et al. 2011; Rogers et al. 2005; Hanson et al. 2009; Chawla et al. 2009). In addition, a rolling validation study is being conducted by NCEP, which currently covers only the Hawaiian Islands and Alaska within our study region from 2008 to 2010. The studies are conducted for limited periods and a limited number of buoys in the Pacific. Most studies validate only the significant wave height, except for Hanson et al. (2009) and Chawla et al. (2009), which also validate the dominant wave period against buoy data. The study periods range from a few weeks to 4 years and the longer ones provide seasonal bias pattern information. All of these studies showed that the model performs well against observed data. In Pacific basin hindcasts, WW3 performed better than third-generation wave prediction model, cycle 4.5 (WAM 4.5), and second-generation wave model, version 4c (WAVAD 4c; Hanson et al. 2009). None of these studies, however, address the wave-generation response to the hurricane force cyclones specifically, nor the capability of WW3 to forecast large waves.

The motivation for this study is to draw attention to and help promote mitigation of the hazard created by HF extratropical cyclones to marine shipping and coastal interests. First, the climatology of captured fetches associated with HF storms was constructed. Second, a comparison between QuikSCAT wind observations and GDAS analysis of the winds was performed. Third, the wave response to these strong storms was documented in buoy data and compared to WW3 hindcasts.

## 2. Methodology and data

QuikSCAT data were obtained from Remote Sensing Systems (RSS; <http://www.remss.com/missions/qscat>; Wentz and Smith 1999; Ricciardulli and Wentz 2011). For this study, the latest version (4) of QuikSCAT data is used. This version was released in April 2011 after a complete reprocessing using RSS's new Geophysical

Model Function (GMF) Ku-2011, which was developed with special attention to high winds. The QuikSCAT polar-orbit satellite provides wind measurements over 90% of the earth's ice-free ocean daily (in 24 h) with errors of less than  $2 \text{ m s}^{-1}$  in speed and  $20^\circ$  in direction (Hoffman and Leidner 2005). The 1800-km swath has a nominal spatial resolution of  $0.25^\circ \times 0.25^\circ$  to capture mesoscale winds (e.g., Fig. 1). Yuan (2004) has shown that relatively accurate retrievals of extreme winds can be obtained with this instrument.

In this study, the extent of captured fetches with winds  $>18 \text{ m s}^{-1}$  [35 knots (kt;  $1 \text{ kt} = 0.51 \text{ m s}^{-1}$ )] were documented for each of the winter HF extratropical cyclones that occurred in the North Pacific Ocean over a 6-yr period (2003–08). Each storm included in this study has at least one synoptic time during which hurricane force winds were observed. For this study, a captured fetch is defined as the open-water area over which the wind blows in the same direction as the storm system motion (Bigelow and Edmondson 1947; Butt et al. 2014). A total of 197 HF storms were tracked, and captured storm fetches were identified using the QuikSCAT data. Winds of at least gale force ( $>34 \text{ kt}$  or  $17.5 \text{ m s}^{-1}$ ) can generate large waves (Bigelow and Edmondson 1947; Morris and Nelson 1977). Gale force winds coupled with fetches of 300 nautical miles (n mi;  $1 \text{ n mi} = 1.852 \text{ km}$ ) may generate swells of 8.4 m ( $\sim 28 \text{ ft}$ ) (Bigelow and Edmondson 1947).

The fetch extent, indicated by polygons, at each synoptic time was objectively determined based on the presence of wind vectors of at least gale force pointed within  $\pm 10^\circ$  of the direction of the storm motion. Individual fetches were then superimposed using Adobe Illustrator. Captured fetches produce larger swells, other factors being equal, because higher winds continue to blow over the area of the propagating swell. Wider fetches result in less angular spreading and, thus, larger swell propagation (Butt et al. 2014). Gaps between the fetches either correspond to evolving winds dropping below the gale wind threshold of 34 kt or missing or unavailable QuikSCAT data for a particular storm and a particular synoptic time.

To investigate how El Niño–Southern Oscillation (ENSO) impacts the distribution of captured fetches in HF storms, data from an El Niño and a La Niña year were plotted separately for the period December–March, when the impact of ENSO on the weather over the North Pacific Ocean is most pronounced (Chu and Chen 2005).

In the state of Hawaii, 25 ft ( $\sim 7.5 \text{ m}$ ) is the threshold for a high surf warning on the northern shores of the islands. To estimate the wave response in the Hawaii surfzone from deep-water significant wave heights and

peak periods, Caldwell and Aucan (2007) developed an empirical formula for the North Shore of Oahu:

$$H_b = K_r H_s P,$$

where  $H_b$  = breaker height,  $H_s$  = significant wave height,  $P$  = wave period, and  $K_r$  = refraction coefficient or shoaling factor (per period). In this formula,  $H_b$  is the maximum height of the wave face just prior to breaking at the coast and provides a convenient gauge of the coastal hazard of open-ocean swell conditions. The shoaling factor, or refraction coefficient, in the formula was empirically derived using directional buoy data collected just offshore of Waimea Bay and wave-height estimates made by professional lifeguards at Sunset Beach, Banzai Pipeline, and Waimea Bay on the North Shore of Oahu (Caldwell and Aucan 2007). Their analysis found that the shoaling factor for the North Shore of Oahu was 0.12 for the surf break Pipeline and generally 0.1 for the North Shore (P. Caldwell 2009, personal communication). In this study, Caldwell and Aucan's approach was adopted with a shoaling factor value of 0.1 applied as an estimate of average bathymetry conditions over the domain of the study. Scatterplots of observed versus forecast breaker height and dominant wave period were plotted for HF storm cases that began when the surf-warning threshold conditions with breaker height of 25 ft (7.5 m) were first exceeded at a buoy and ended when the waves began to diminish.

Buoy observations were obtained from NOAA's National Data Buoy Center (NDBC). Wave spectra from the NDBC stations are computed hourly from 20-min records. The buoys included in this study are located off the coasts of Alaska, Washington, Oregon, California, and Hawaii and are sufficiently widely distributed to reflect effects from a broad range of wave-generating fetches (Fig. 2). Because wind waves follow great-circle routes, these routes were used to identify which buoys would be impacted by the wind waves. The deep-water wave propagation formula was used to estimate the arrival time of the swell at respective buoys, using WW3 output for the wavelength of the dominant swell.

Additionally, this study accessed data from the Global Data Assimilation System (GDAS) analyses. GDAS 6-hourly wind-velocity data with  $1^\circ \times 1^\circ$  grid spacing and at 6-h intervals are available from NOAA/National Climatic Data Center (NCDC).

In this study, hindcast data from the global WW3 and data from the Alaska Waters (AKW) and Eastern North Pacific (ENP) regional WW3 were used. To drive the waves, the WW3 requires ice concentration and winds (including the air–sea temperature difference) as input fields. Winds from the GDAS analyses, converted to 10-m

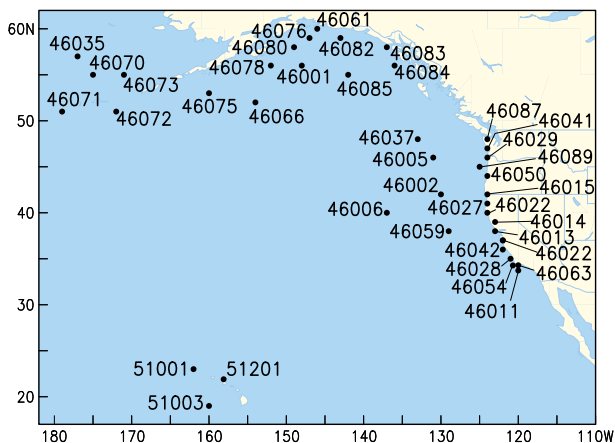


FIG. 2. NOAA buoy locations and numbers used in this study.

height, are used as input for continuous WW3 hindcasts. The model predicts waves that are directly generated by wind from deep to intermediate water, outside the surfzone. Version 2.22 of WW3, with a resolution of  $1.25^\circ \times 1^\circ$ , was employed at NCEP to regenerate the historical data archive used in this study.

### 3. Results

#### a. A brief case study

The case study presented in this section documents the winds and sea state (Figs. 3 and 4) during storm 37 of the 2006/07 storm season. The storm traveled from Japan to Alaska, generating large waves at both the Hawaii and Alaska coasts. Captured fetches associated with this storm are highlighted (in red in Fig. 6, described in greater detail below). Storm 37 generated the largest open-ocean waves observed at the Hawaii buoys during the study period: 7.3 m at 0100 UTC 30 January with a wave period of 14.8 s at buoy 51001 off of Kauai. The storm also generated a wave that was measured at 12.3 m with a dominant wave period of 14.3 s at 2300 UTC 30 January by Alaska buoy 46075. This was the fourth-largest open-ocean wave throughout the entire study period and study region as observed by the buoys.

A comparison of the wind field observed by QuikSCAT to that estimated in the GDAS analysis shows that the QuikSCAT winds are not accurately reflected in the GFS initial conditions (Fig. 3). Both the location ( $\sim 8^\circ$ , too far to the west) and the magnitude ( $16 \text{ m s}^{-1}$ , too low) of the wind maximum have errors in the GDAS analysis. Some of the wind-velocity discrepancy may be an issue of the grid spacing of the two datasets,  $1^\circ$  versus  $0.25^\circ$ , but the large location error cannot be explained by this difference in resolution. In the case of Alaska buoy 46075, the maximum breaker height was 19.7 m, whereas the breaker height hindcast by WW3 was 12.0 m, for an error

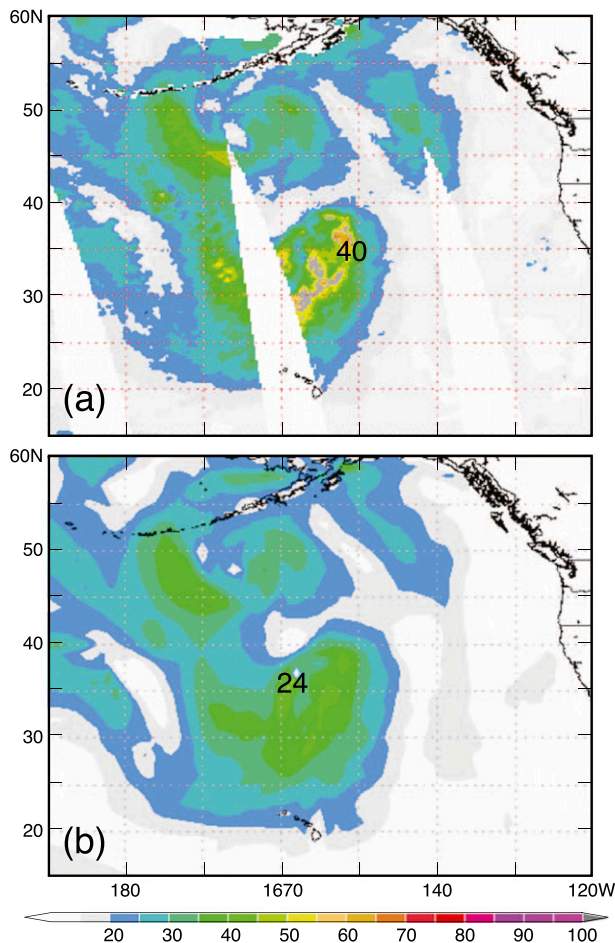


FIG. 3. Wind speed ( $\text{m s}^{-1}$ ) at 0600 UTC 29 Jan 2007 when the fetch of storm 37 was pointing toward Hawaii: (a) observed by QuikSCAT and (b) from the GDAS analysis. Gray areas in (a) indicate rain contamination.

of 7.7 m (Fig. 4). The kinetic energy imparted by a breaking wave goes as the square of the wave height. The results of this case study are consistent with those of Chelton et al. (2006), who showed that the operational GDAS considerably underestimated the intensity of an HF cyclone over the North Pacific on 10 January 2005 (storm 14 of the 2004/05 season).

#### b. Storm fetch climatology

Maps of captured fetches associated with HF storms from 2003 to 2008 show significant interannual variability spatially and in number (Figs. 5 and 6). Observations show that HF extratropical cyclones do not occur during the months of June–August. There are 21 HF storms in 2003/04 (Fig. 5a), increasing to 30 storms in 2004/05 (Fig. 5b). In 2005/06, there is a slight increase with a total of 33 storms (Fig. 5c). During El Niño year 2006/07 and La Niña year 2007/08, 35 HF storms were documented between December and March (Fig. 6). Storms 44 and 45 are shown in Fig. 1.

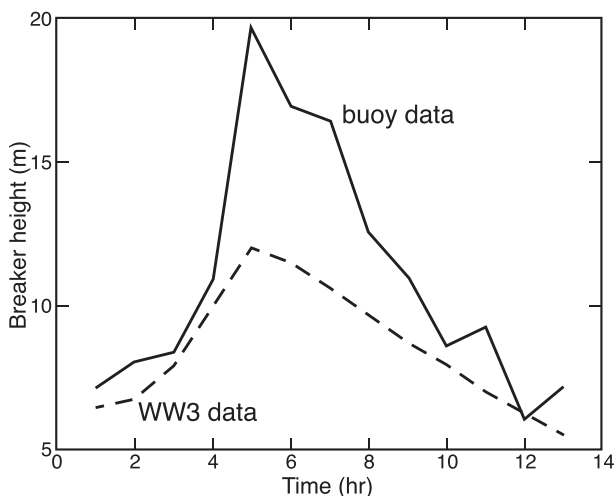


FIG. 4. Evolution of wave-height conditions for storm 37 (2007) as observed by buoy 46075 on the Alaska coast and as forecast by WW3 from initial conditions at 1200 UTC 30 Jan. In the plot, time = 1 h is 1200 UTC 30 Jan, and time = 13 h is 0000 UTC 1 Feb.

The zone of greatest hazard from a large swell is represented by the darkest (densest) region on the maps. The location of the wave hazard zone shifts from year to year, while the area covered by the wave hazard expands and shrinks. A clustering of fetches is seen in the northeastern Pacific in 2003/04 (Fig. 5a). The hazard zone shifts southeast to the mid-Pacific in 2004/05, and covers a larger area than in 2003/04. In 2005/06, the hazard zone shifts westward and is denser than both previous years (Fig. 5c).

During an El Niño year, the high hazard zone shifts westward compared to a La Niña year (Fig. 6). In addition, the hazard zone is denser compared to La Niña, during which the HF storm fetches are more broadly distributed. Although the statistical significance of the observed shift in storm fetches cannot be evaluated with data from only one ENSO cycle, these results are consistent with the literature on the well-known Pacific–North American (PNA) teleconnection pattern between equatorial Pacific sea surface temperature anomalies and Rossby waves that determine storm tracks (Horel and Wallace 1981; Seager et al. 2010).

Superimposing all the HF storm fetches during the period of this study showed that the zone of greatest captured fetch density encompassed an area from about 30° to 45°N and from 155°E to 190°W (Fig. 7a). The result seen in Fig. 7a is consistent with the distribution of a very large swell (>12m open-ocean waves) detected by satellite altimeter data (Fig. 7b) (Cardone et al. 2015).

Most HF storms track in an easterly direction. Therefore, the majority of captured fetches direct large swells toward southwestern Alaska, including the

Aleutians, and southeastern Alaska. The Canadian coast and the Northwest United States also receive a large fraction of the storm swells. Exceptions occur when storms adopt a northerly or northwesterly direction of motion during their dissipating stage. It is not uncommon to have the surface low center begin to track in an increasingly northerly and then northwesterly direction as the storms occlude. This is in part the result of forcing by vorticity maxima aloft associated with the occlusion cloud band (Businger and Reed 1989). As the surface low center approaches higher pressure to the north, the pressure gradient on the north side of the low increases, resulting in enhanced easterly winds.

During El Niño year 2006/07, there are more storms heading in the southeast direction, extending captured fetches into the subtropics south of 30°N. Both of these conditions tend to produce large swells for the Hawaiian Islands (Fig. 6a). The El Niño year also saw more captured fetches directing swells toward the east coast of the Russian Federation and the southwestern coast of Alaska.

The width of captured fetches and the distance traveled varied from storm to storm. Some storms traveled across the entire North Pacific before dissipating, such as storms 37 and 38 of 2006/07, which spun up in the northwestern Pacific off the eastern coast of Japan and dissipated in the northeastern Pacific (Fig. 6a). Other storms traveled a relatively short distance, such as storm 25 off the coast of California (Fig. 6a). Cyclone families were observed during the study period where the subsequent cyclones tend to follow a track just north of the preceding cyclone (Bjerknes and Solberg 1922). Storms 36–38 (Fig. 6a) and 47 and 48 (Fig. 6b) are examples of this phenomenon.

A combination of a long coastline and exposure makes Alaska the state most prone to hazardous swells generated by HF extratropical cyclones (Fig. 8). The total numbers of surf-warning threshold conditions received by state are 143 in Alaska, 48 in Washington, 28 in Oregon, 46 in California, and 7 in Hawaii. Washington and California are nearly tied for wave impacts. Hawaii, because of its tropical location and large numbers of ocean users, suffers a disproportionate number of fatalities due to high surf (R. Tanabe, NWSFO Honolulu, 2013, personal communication).

### c. Comparison of observed and modeled data

A total of 833 comparisons between QuikSCAT and GDAS-analyzed wind maxima in captured fetches show an increased underestimation of the wind speed in the GDAS analyses with increased wind speed (Fig. 9). As pointed out previously, some of the difference may be because of the larger grid spacing in the GDAS analyses than in the QuikSCAT data (1° versus 0.25°). However, the

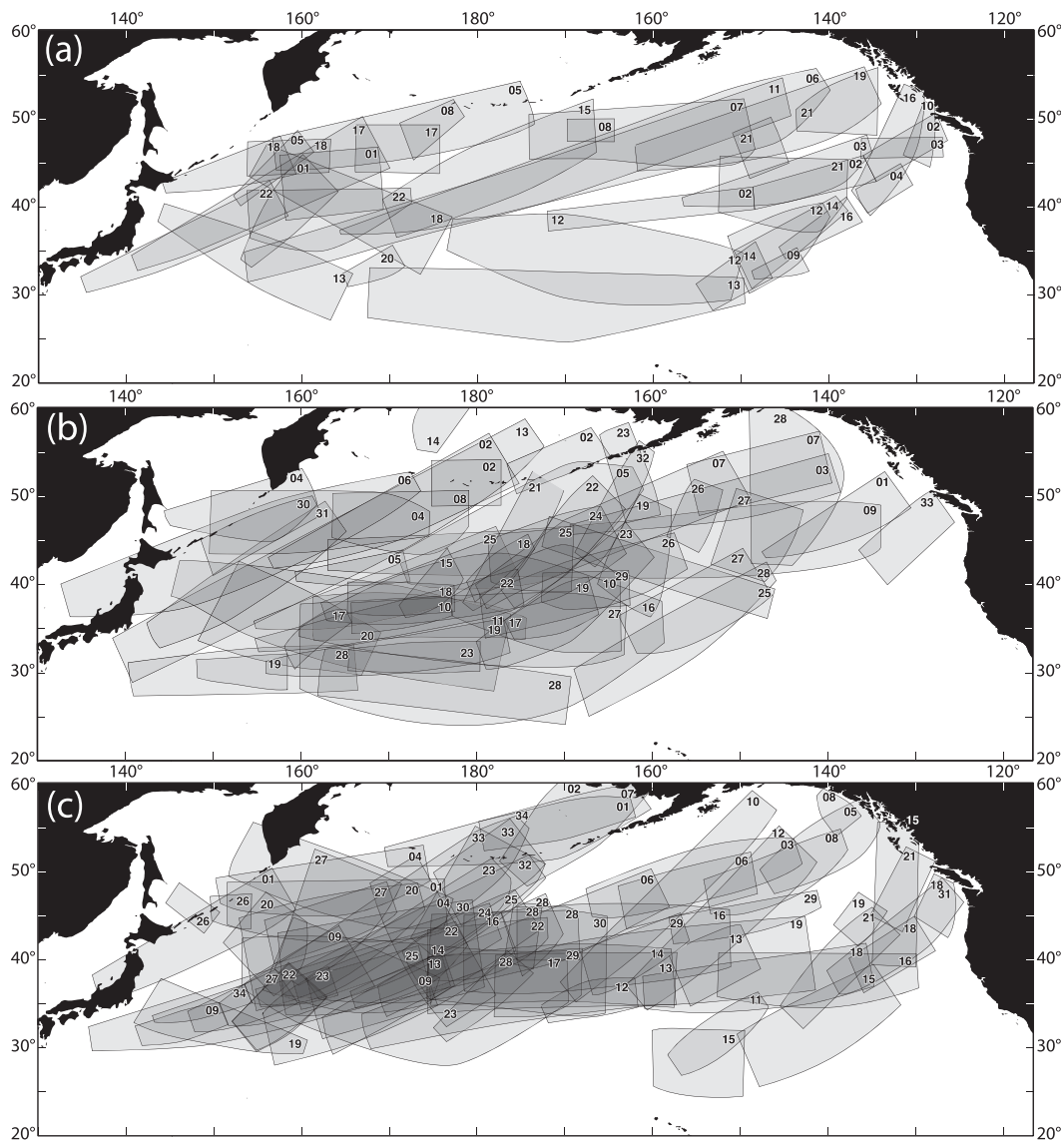


FIG. 5. Captured fetches (gray polygons) determined for the HF extratropical cyclones for the storm season from September to May (a) 2003/04, (b) 2004/05, and (c) 2005/06. Numbers give the chronological order (within each season) of the storm that produced the fetch and are plotted at the end of the fetch toward which the wind is blowing. Note that captured fetches may be found for multiple synoptic times for a single storm, with breaks between polygons indicating changing wind direction or data gaps.

resolution difference does not explain all of the discrepancy, and it is suggested that some of the discrepancy is because of a low bias in the GDAS analysis, especially at higher winds speeds. The nonlinear impact of wind forcing on the sea surface amplifies the error in the generation of wind waves (Businger and Businger 2001).

A case study analysis of WW3 (not shown) and previous research shows that wave steepness is greatest in the core of the fetches and greater than the damage threshold for ships (0.03) (Toffoli et al. 2005). A total of 278 threshold-exceeding cases were identified based on buoy data. A comparison between WW3 hindcasts and

buoy observations of breaker height and dominant wave period shows that the model underestimates both for larger swells (Fig. 10). The WW3 tends to underestimate  $H_b$  after approximately 6 m (Fig. 10a). There are a few cases where the difference between the WW3 output and observations suggests that the model hindcast missed the swell completely. This could be the result of poor wind strength and/or wind direction data in the GDAS initial conditions passed to WW3. The linear fit for waves larger than 6 m indicates that the larger the wave, the greater the WW3's tendency to underestimate wave height. Similar observations hold true in the case of dominant or peak

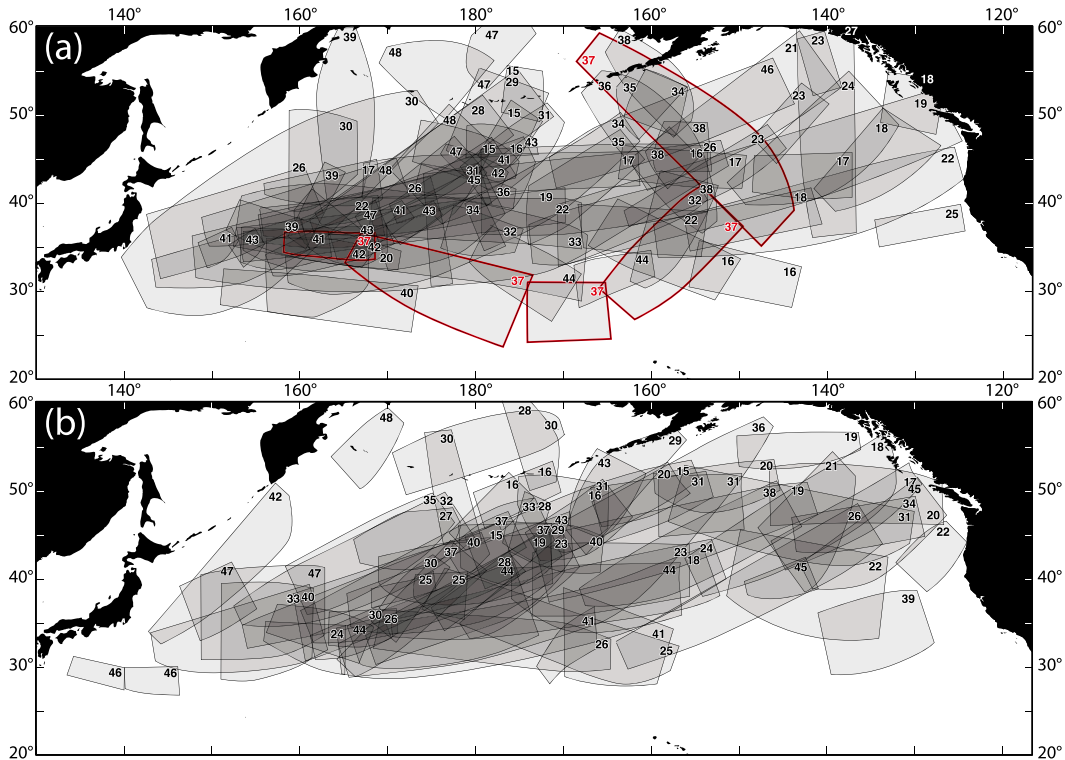


FIG. 6. Captured fetches determined for the part of the storm season from December to March (a) 2006/07 during an El Niño event and (b) 2007/08 during a La Niña event. See the Fig. 5 caption for an explanation of the plot. Fetches outlined in red are associated with storm 37, whose buoy wave heights are shown in Fig. 4.

wave periods (Fig. 10b). Above  $\sim 9$  s, WW3 increasingly underestimates the wave period.

#### 4. Conclusions and discussion

The goal of this study was to better understand the relationship between HF winds in extratropical cyclones documented by QuikSCAT and the resulting open-ocean and coastal hazards. The study verifies that extreme surface winds produced by extratropical cyclones are frequently observed over the oceans during winter. Their occurrence is often accompanied by extreme wave conditions, representing a major threat to the safety of marine operations and coastal communities. Therefore, the crucial challenge is to produce accurate guidance on the likelihood and characteristics of severe sea state conditions. Therefore, it is noteworthy that production of accurate guidance on the likelihood and characteristics of severe sea state conditions remains a challenge. This is due in part to inadequacies in the operational analyses of ocean surface wind conditions in these extreme storms. In particular, analyses from NCEP are characterized by a substantial underestimation of surface winds in intense storms, despite the fact that satellite observations of ocean surface winds are assimilated. Because of the underestimation of extreme surface wind fields, dangerous wave events are also

underestimated. Part of the challenge is that assimilation systems are currently unable to assimilate surface observations strongly in regions with few upper-air observations.

##### a. Conclusions

- Case studies and statistical analysis suggest that the GDAS wind analyses underestimate the strength of the winds in HF storms when compared to QuikSCAT satellite wind observations, with the error increasing with increasing wind speed.
- NOAA buoy observations show that the WW3 underforecasts large wave events over the North Pacific Ocean, consistent with the underanalyzed winds.
- Maps of captured storm fetches document the areal extent of greatest hazard and the degree of interannual variability.
- The composite map of captured fetch hazard is consistent with the satellite altimeter analysis of large wave events (Cardone et al. 2015).
- The WW3 wave steepness is greatest in the core of the captured fetches and exceeds the steepness threshold of 0.03 associated with damage for ships.
- The results of this study suggest that a QuikSCAT-type instrument represents an important resource for surface wind data.



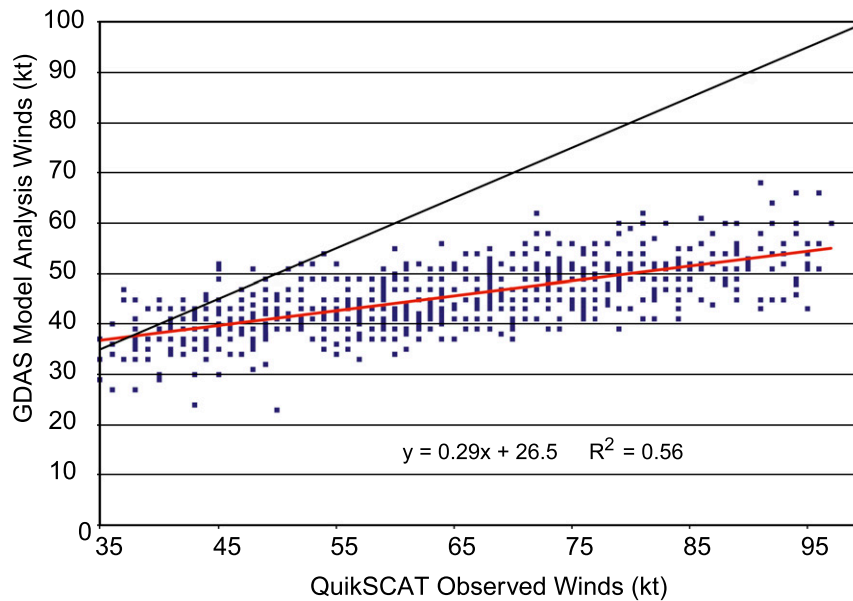


FIG. 9. Comparison of the QuikSCAT and GDAS-analyzed wind maxima between 2003 and 2008.

showed that blending QuikSCAT winds in the hindcast process notably reduced the model significant wave-height bias. As WW3 is forced with assimilated surface winds from GDAS, under- or overestimated wind input will cause under- or overforecasting of wind waves. Chelton et al. (2006) showed that the QuikSCAT is underutilized by the NCEP GDAS.

In the case study of the 29 January 2007 storm over the North Pacific, GDAS considerably underestimated the intensity of the cyclone. At 0600 UTC, the maximum wind predicted in GDAS was  $24 \text{ m s}^{-1}$  while the maximum wind speed measured by the satellite was  $40 \text{ m s}^{-1}$ , a large error of  $16 \text{ m s}^{-1}$ . The GDAS analysis showed only gale force winds, while the winds were at hurricane force in the QuikSCAT observations. The large underestimation in the analysis is despite the fact that QuikSCAT data were assimilated in the model. This leads to the conclusion that the tendency of WW3 to underestimate large waves shown in the results can be attributed in part to the fact that the QuikSCAT winds were not assimilated well enough, and that the current lack of QuikSCAT data could possibly lead to even larger present-day biases in wind-wave prediction. Data from the Advanced Scatterometer (ASCAT), which are less affected by rain (C band versus Ku band), are being assimilated but the spatial coverage is not as good as that of QuikSCAT (Figa-Saldaña et al. 2002). It should be noted that the assimilation of surface winds over the open ocean is made more challenging by the lack of in situ upper-air data in these same areas.

Underforecast storm winds also pose a significant problem for coastal areas when HF storms make land-fall, producing significant coastal flooding and widespread power outages (McMurdie and Mass 2004; Chang et al. 2009). The Pacific Northwest is a region particularly vulnerable to strong cyclone-based windstorms because of its unique vegetation and terrain (Mass and Dotson 2010). The December 2006 Hanukkah Eve HF extratropical cyclone destroyed thousands of acres of trees, knocked out power for  $\sim 1.5$  million customers, damaged hundreds of structures and homes, and injured dozens of people in the U.S. Pacific Northwest and British Columbia, Canada (Chang et al. 2009). The storm produced the most damaging winds since 1962, with winds gusting to  $40\text{--}45 \text{ m s}^{-1}$  along the coast leading to the fatalities of at least 13 people, highlighting the need for accurate ocean observations and model forecasts (Mass and Dotson 2010).

Analysis of a global ship accident database by Toffoli et al. (2005) using wave model hindcast results revealed that three out of five cases occurred during sea states characterized by wave steepness between 0.03 and 0.045, and two out of three incidents occurred during a sea state with significant wave height lower than 4 m. Maximum wave steepness values observed during the storm development in the case study presented here were consistently higher than those estimated for the ship accidents. The same holds true for wave height, which suggests that sea states in the North Pacific Ocean under conditions of HF extratropical cyclones pose a tangible

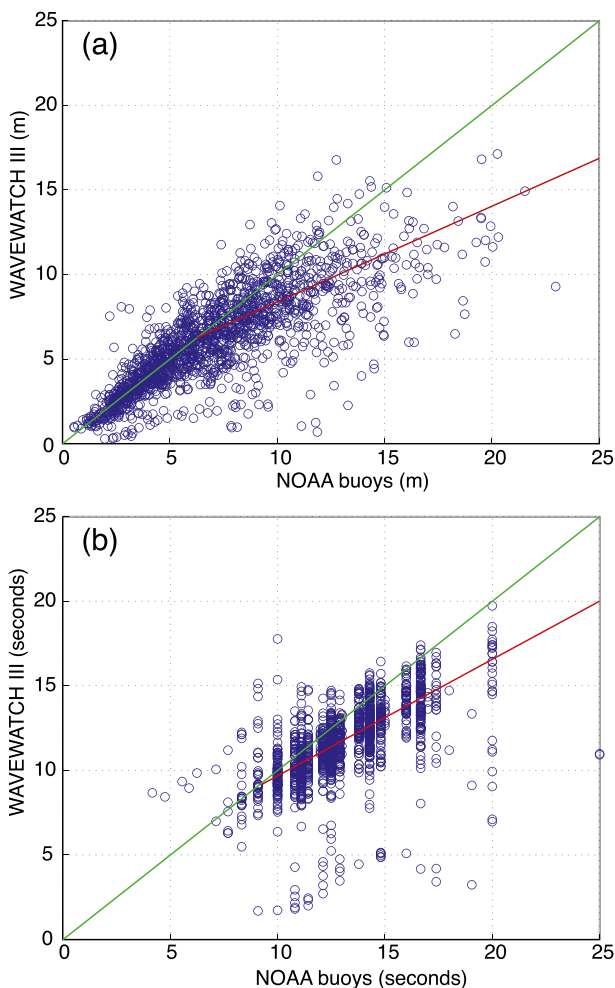


FIG. 10. Comparison of WW3-estimated and buoy-observed (a)  $H_b$  and (b) dominant wave period for all HF storms between 2003 and 2008. Regression value and equation are shown in Fig. 9.

threat to maritime safety. Steeper seas yield dangerous dynamic impacts to ship motion, such as slamming (Toffoli et al. 2005). Synchronous ship motion (pitch and roll), which is likely even in moderately high waves, can be extremely hazardous for container ships (Hua and Wang 2001). When the roll period of the ship is the same as that of the wave, the ship's rolling motion can build up to a large amplitude in a few wave periods, a phenomenon known as excited roll motion. All of these issues make the accurate forecasting of wave height and wave period by wind-wave models such as WW3 critical for maritime safety.

The storm fetch climatology presented here suggests where the greatest occurrence of hazardous large swell is concentrated and how the pattern varies from year to year and during the ENSO cycle. Cyclone families were repeatedly observed in the fetch climatology period. These families have considerable implications for

marine safety. Serial temporal clustering of extratropical cyclones, a mechanism that can be explained by cyclone families, was a major cause of insured marine losses in the North Atlantic (Mailier et al. 2006).

The results of the WW3 validation study indicate that the model significantly underestimates large waves and long-wave periods. This result does not match the findings by other validation studies where the model performed well against buoy observations (Tolman 2002a; Stopa et al. 2011; Rogers et al. 2005; Chawla et al. 2009). Chawla et al. (2009) showed that the sign of the significant wave-height bias in the WW3 model depended on whether the compared waves were in the wind-seas (waves under the influence of winds), young swell, or mature swell phase. The model displayed an overall tendency to overestimate wave heights over the northeastern Pacific, a swell-dominated area, which was not the case in our findings, presumably because our study is focused on the strongest wind events. Chawla et al. (2009) also showed that the model does a slightly better job at predicting wave period than wave heights, while the opposite held true in our findings. Tolman (2002a) evaluated the effects of model changes from WW3 versions 1.18–2.22 and showed that incorporating subgrids to resolve islands had a significant impact in the model's forecasting ability in Alaska and Hawaii, because of the model's ability to more accurately capture shadowing and refraction of waves by islands. Overall, the model underestimated the significant wave heights in the global run when subgrids were incorporated, a trend observed in the results presented here.

Although operational wave modeling has been successful overall in the past decades, there are many unresolved scientific issues pertaining to wave forecasting (Tolman 2008). Wind-wave propagation in deep water over large distances is complicated by a phenomenon known as the garden sprinkler effect (GSE). GSE occurs because spectral resolution in direction is sufficiently coarse so that spatial propagation of discrete directions results in discrete disintegration of a swell field that should be continuous (Booij and Holthuijsen 1987). Therefore, spatial propagation is a difficult process to model numerically, and although GSE can be alleviated, it is not yet truly solved. Inaccuracies that occur during swell dispersion can be significant in WW3 (Rogers et al. 2005). Inaccuracy in the spectral distribution of low-frequency wave energy leads to inaccuracies as the low-frequency wind sea (waves still under the influence of winds) disperses as a swell. While the total energy of wind-seas wave height is well predicted by the model physics, when given accurate forcing, the frequency and in particular the directional distribution of wave spectra have not been extensively validated. Chawla et al. (2009)

also speculated that underpredicting wave growth in the wind seas leads to underprediction of swells.

The science of modeling wave physics is less developed than modeling wave propagation (Tolman 2008). The basic physics package in a wave model consists of the deep-water input (e.g., winds), nonlinear interactions, and dissipation or white capping. Hanson et al. (2009) suspect that the dissipation term, wave-wave interaction, and atmospheric drag coefficient as part of the wind input source term are likely contributors to swell height error and that significant model improvements are not possible until these terms are improved. Chawla et al. (2009) point out the inability of WW3 to dissipate the energy fast enough once it is transferred to the swell from wind seas.

### c. Future work

The results of this study suggest that there is an opportunity to improve GDAS and WW3 model performance associated with HF cyclones. Because the production of wind retrievals from QuikSCAT ended on 19 November 2009, ocean wind-vector products now rely on the more recent microwave scatterometers, including *Satellite for the Ocean-2* (*OceanSat-2*) Scanning Scatterometer (OSCAT), Ku band (Chakraborty et al. 2013), ASCAT-A and -B C-band (Figa-Saldaña et al. 2002), and the WindSat polarimetric radiometer (Gaiser et al. 2004). In addition, the International Space Station (ISS) Rapid Scatterometer instrument, which is essentially a replica of the QuikSCAT instrument, is currently flying aboard the ISS to measure the earth's ocean surface wind speed and direction. The inclination of the orbit of the ISS is 51.6°; therefore, the coverage is not global. Given these satellite resources, there is an opportunity to further investigate the performance of the GFS and WW3 models utilizing data from these instruments. A significant effort is warranted to improve the assimilation of satellite-derived surface winds into operational NWP models, with the resulting improvement in wind forcing available for global wave prediction models.

*Acknowledgments.* We are grateful to Joseph M. Sienkiewicz of the NOAA/Ocean Prediction Center, who stimulated this research project by providing a list of extratropical cyclones that produced hurricane force winds in QuikSCAT data and was also kind enough to provide constructive feedback on a draft of the manuscript. QuikSCAT data were produced by Remote Sensing Systems and sponsored by the NASA Ocean Vector Winds Science Team. Data are available online ([www.remss.com](http://www.remss.com)). We are grateful to Nancy Hulbert who helped draft the figures. Finally, we are grateful for the thoughtful and thorough comments from two anonymous

reviewers. This work was supported by NOAA under Cooperative Agreement NA11NMS4320128 and the Office of Naval Research under Grant N000140810450.

### REFERENCES

- Bigelow, H. B., and W. T. Edmondson, 1947: *Wind Waves at Sea, Breakers and Surf*. U.S. Department of the Navy, 177 pp.
- Bjerknes, J., and H. Solberg, 1922: Life cycle of cyclones and the polar front theory of atmospheric circulation. *Geophys. Publ.*, **3**, 3–18.
- Booij, N., and L. H. Holthuijsen, 1987: Propagation of ocean waves in discrete spectral wave models. *J. Comput. Phys.*, **68**, 307–326, doi:10.1016/0021-9991(87)90060-X.
- Businger, S., and R. J. Reed, 1989: Cyclogenesis in cold air. *Weather Forecasting*, **4**, 133–156, doi:10.1175/1520-0434(1989)004<0133:CICAM>2.0.CO;2.
- , and J. A. Businger, 2001: Dissipation of turbulence kinetic energy in storms. *J. Atmos. Sci.*, **58**, 3793–3796, doi:10.1175/1520-0469(2001)058<3793:VDOTKE>2.0.CO;2.
- Butt, T., P. Russell, and R. Grigg, 2014: *Surf Science: An Introduction to Waves and Surfing*. 3rd ed. Alison Hodge Press, 178 pp.
- Caldwell, P. C., and J. P. Aucan, 2007: An empirical method for estimating surf heights from deepwater significant wave heights and peak periods in coastal zones with narrow shelves, steep bottom slopes, and high refraction. *J. Coastal Res.*, **23**, 1237–1244, doi:10.2112/04-0397R.1.
- Cardone, V. J., B. T. Callahan, H. Chen, A. T. Cox, M. A. Morrone, and V. R. Swail, 2015: Global distribution and risk to shipping of very extreme sea states (VESS). *Int. J. Climatol.*, **35**, 69–84, doi:10.1002/joc.3963.
- Chakraborty, A., R. Kumar, and A. Stoffelen, 2013: Validation of ocean surface winds from the *OceanSat-2* scatterometer using triple collocation. *Remote Sens. Lett.*, **4**, 85–94, doi:10.1080/2150704X.2012.693967.
- Chang, P. S., Z. Jelenak, J. M. Sienkiewicz, R. Knabb, M. J. Brennan, D. G. Long, and M. Freeberg, 2009: Operational use and impact of satellite remotely sensed ocean surface vector winds in the marine warning and forecasting environment. *Oceanography*, **22**, 194–207, doi:10.5670/oceanog.2009.49.
- Chawla, A., H. L. Tolman, J. L. Hanson, E.-M. Devaliere, and V. M. Gerald, 2009: Validation of a multi-grid WAVEWATCH III modeling system. *Proc. 11th Waves Hindcasting and Forecasting Workshop*, Halifax NS, WMO-JCOMM. [Available online at [http://www.waveworkshop.org/11thWaves/Papers/multi\\_hindanalysis.pdf](http://www.waveworkshop.org/11thWaves/Papers/multi_hindanalysis.pdf).]
- Chelton, D. B., M. H. Freilich, J. M. Sienkiewicz, and J. M. Von Ahn, 2006: On the use of QuikSCAT scatterometer measurements of surface winds for marine weather prediction. *Mon. Wea. Rev.*, **134**, 2055–2071, doi:10.1175/MWR3179.1.
- Chu, P.-S., and H. Chen, 2005: Interannual and interdecadal rainfall variations in the Hawaiian Islands. *J. Climate*, **18**, 4796–4813, doi:10.1175/JCLI3578.1.
- Dickinson, S., and R. A. Brown, 1996: A study of near-surface winds in marine cyclones using multiple satellite sensors. *J. Appl. Meteor.*, **35**, 769–781, doi:10.1175/1520-0450(1996)035<0769:ASONSW>2.0.CO;2.
- Ebuchi, N., H. C. Graber, and M. J. Caruso, 2002: Evaluation of wind vectors by QuikSCAT/SeaWinds using ocean buoy data. *J. Atmos. Oceanic Technol.*, **19**, 2049–2062, doi:10.1175/1520-0426(2002)019<2049:EOWVOB>2.0.CO;2.

- Figa-Saldaña, J., J. J. W. Wilson, E. Attema, R. Gelsthorpe, M. R. Drinkwater, and A. Stoffelen, 2002: The Advanced Scatterometer (ASCAT) on the Meteorological Operational (MetOp) platform: A follow on for European wind scatterometers. *Can. J. Remote Sens.*, **28**, 404–412, doi:10.5589/m02-035.
- Gaiser, P. W., and Coauthors, 2004: The WindSat spaceborne polarimetric microwave radiometer: Sensor description and early orbit performance. *IEEE Trans. Geosci. Remote Sens.*, **42**, 2347–2361, doi:10.1109/TGRS.2004.836867.
- Hanson, J. L., B. A. Tracy, H. L. Tolman, and R. D. Scott, 2009: Pacific hindcast performance of three numerical wave models. *J. Atmos. Oceanic Technol.*, **26**, 1614–1633, doi:10.1175/2009JTECHO650.1.
- Hoffman, R. N., and S. M. Leidner, 2005: An introduction to the near-real-time QuikSCAT data. *Wea. Forecasting*, **20**, 476–493, doi:10.1175/WAF841.1.
- Horel, J. D., and J. M. Wallace, 1981: Planetary-scale atmospheric phenomena associated with the Southern Oscillation. *Mon. Wea. Rev.*, **109**, 813–829, doi:10.1175/1520-0493(1981)109<0813:PSAPAW>2.0.CO;2.
- Hua, J., and W. H. Wang, 2001: Roll motion of a ro-ro-ship in irregular following waves. *J. Mar. Sci. Technol.*, **9**, 38–44.
- Izaguirre, C., F. J. Méndez, M. Menéndez, and I. J. Losada, 2011: Global extreme wave height variability based on satellite data. *Geophys. Res. Lett.*, **38**, L10607, doi:10.1029/2011GL047302.
- Jelenak, Z., and P. S. Chang, 2008: NOAA operational satellite ocean surface vector winds—QuikSCAT follow-on mission: User impact study. NOAA Tech. Rep., 90 pp. [Available online at [http://manati.orbit.nesdis.noaa.gov/SVW\\_nextgen/QFO\\_user\\_impact\\_study\\_final.pdf](http://manati.orbit.nesdis.noaa.gov/SVW_nextgen/QFO_user_impact_study_final.pdf).]
- , K. Ahmad, J. Sienkiewicz, and P. S. Chang, 2009: A statistical study of wind field distribution within extra-tropical cyclones in North Pacific Ocean from 7-years of QuikSCAT wind data. *Proc. Int. Geoscience and Remote Sensing Symp.*, Vol. 1, Cape Town, South Africa, IEEE, doi:10.1109/IGARSS.2009.5416931.
- Kite-Powell, H. L., 2011: The value of ocean surface wind information for maritime commerce. *Mar. Technol. Soc. J.*, **45**, 75–84, doi:10.4031/MTSJ.45.1.13.
- Mailier, P. J., D. B. Stephenson, C. A. T. Ferro, and K. I. Hodges, 2006: Serial clustering of extratropical cyclones. *Mon. Wea. Rev.*, **134**, 2224–2240, doi:10.1175/MWR3160.1.
- Mass, C., and B. Dotson, 2010: Major extratropical cyclones of the Northwest United States: Historical review, climatology, and synoptic environment. *Mon. Wea. Rev.*, **138**, 2499–2527, doi:10.1175/2010MWR3213.1.
- McMurdie, L., and C. Mass, 2004: Major numerical forecast failures over the northeast Pacific. *Wea. Forecasting*, **19**, 338–356, doi:10.1175/1520-0434(2004)019<0338:MNFOT>2.0.CO;2.
- Morris, V., and J. Nelson, 1977: *The Weather Surfer*. Grossmont Press, 103 pp.
- Ricciardulli, L., and F. Wentz, 2011: Reprocessed QuikSCAT (V04) wind vectors with Ku-2011 Geophysical Model Function. Remote Sensing Systems Tech. Rep. 043011, Santa Rosa, CA, 8 pp.
- Rogers, W. E., P. A. Wittmann, D. W. C. Wang, R. M. Clancy, and Y. L. Hsu, 2005: Evaluations of global wave prediction at the Fleet Numerical Meteorology and Oceanography Center. *Wea. Forecasting*, **20**, 745, doi:10.1175/WAF882.1.
- Sampe, T., and S.-P. Xie, 2007: Mapping high sea winds from space: A global climatology. *Bull. Amer. Meteor. Soc.*, **88**, 1965–1978, doi:10.1175/BAMS-88-12-1965.
- Seager, R., N. H. Naik, M. F. Ting, M. A. Cane, N. Harnik, and Y. Kushnir, 2010: Adjustment of the atmospheric circulation to tropical Pacific SST anomalies: Variability of transient eddy propagation in the Pacific–North America sector. *Quart. J. Roy. Meteor. Soc.*, **136**, 277–296.
- Stopa, J., K. Cheung, and Y. Chen, 2011: Assessment of wave energy resources in Hawaii. *Renewable Energy*, **36**, 554–567, doi:10.1016/j.renene.2010.07.014.
- Toffoli, A., J. M. Lefevre, E. Bitner-Gregersen, and J. Monbaliu, 2005: Towards the identification of warning criteria: Analysis of a ship accident database. *Appl. Ocean Res.*, **27**, 281–291, doi:10.1016/j.apor.2006.03.003.
- Tolman, H. L., 2002a: Testing of WAVEWATCH III version 2.22 in NCEP's NWW3 ocean wave model suite. NOAA/NWS/NCEP/OMB Tech. Note 214, 99 pp.
- , 2002b: User manual and system documentation of WAVEWATCH-III version 2.22. NOAA/NWS/NCEP/OMB Tech. Note 222, 133 pp.
- , 2008: Practical wind wave modeling. *Proc. CBMS Conf. Water Waves: Theory and Experiment*, Howard University, Word Scientific Publishers.
- Von Ahn, J. M., J. M. Sienkiewicz, and G. Mcfadden, 2005: Hurricane force extratropical cyclones observed using QuikSCAT. *Mar. Wea. Log.*, **49**, 34–39.
- , —, and P. S. Chang, 2006: The operational impact of QuikSCAT winds at the NOAA Ocean Prediction Center. *Wea. Forecasting*, **21**, 523–553, doi:10.1175/WAF934.1.
- Wang, X. L., and V. R. Swail, 2001: Changes of extreme wave heights in Northern Hemisphere oceans and related atmospheric circulation regimes. *J. Climate*, **14**, 2204–2221, doi:10.1175/1520-0442(2001)014<2204:COEWHI>2.0.CO;2.
- Wentz, F. J., and D. K. Smith, 1999: A model function for the ocean-normalized radar cross section at 14 GHz derived from NSCAT observations. *J. Geophys. Res.*, **104**, 11 499–11 514, doi:10.1029/98JC02148.
- Willis, M., M. Garces, C. Hetzer, and S. Businger, 2004: Infrasonic observations of open ocean swells in the Pacific: Deciphering the song of the sea. *Geophys. Res. Lett.*, **31**, L19303, doi:10.1029/2004GL020684.
- Yuan, X., 2004: High-wind-speed evaluation in the Southern Ocean. *J. Geophys. Res.*, **109**, D13101, doi:10.1029/2003JD004179.